

# Optimisation of photonic crystal coupling through waveguide design

R. J. E. Taylor<sup>1,2</sup> · P. Ivanov<sup>1,3</sup> · G. Li<sup>1,3</sup> · D. T. D. Childs<sup>1,3</sup> ·  
R. A. Hogg<sup>1,3</sup>

Received: 2 June 2016 / Accepted: 29 December 2016 / Published online: 6 January 2017  
© The Author(s) 2017. This article is published with open access at Springerlink.com

**Abstract** This paper considers multiple structural designs for photonic crystal surface emitting lasers operating at key wavelengths. Initially a structure from Williams et al. is modelled, the structure is modified to include an additional GaAs waveguide layer (termed ballast layer) and to include an additional PC layer (termed double decker). These structures are modelled by a combination of coupling calculation and waveguide modelling and are compared to the original structure. We show that both of these schemes give an increase in coupling, but present fabrication challenges. Next, we model standard laser structures operating at key wavelengths (400 nm, 1.3 and 10  $\mu\text{m}$ ) where a photonic crystal is located above the active region and explore the effect of increasing thickness of photonic crystal. We find that increasing the thickness increases the coupling coefficient but not true for the full range of thicknesses considered. This study allows a more universal comparison of the use of all-semiconductor, or void containing PCSELS to be conducted and we find that the realisation of all semiconductor PCSELS covering a wide range of material and wavelengths are possible.

**Keywords** Photonic crystal · Laser · Waveguide

---

✉ R. J. E. Taylor  
ricjimeee@googlemail.com

<sup>1</sup> Department of Electronic and Electrical Engineering, The University of Sheffield, Sheffield S3 7HQ, UK

<sup>2</sup> Department of Electrical Engineering and Information Systems, School of Engineering, The University of Tokyo, 7-3-Hongo, Bunkyo-ku, Tokyo 113-8656, Japan

<sup>3</sup> School of Engineering, The University of Glasgow, Glasgow G12 8LT, UK

## 1 Introduction

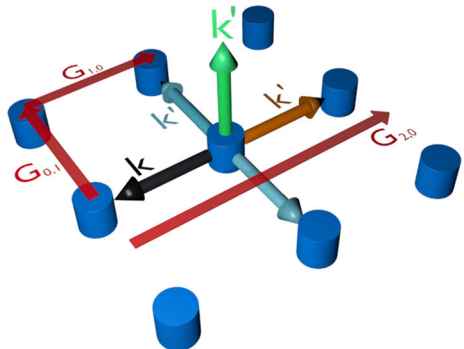
There has been considerable recent interest in photonic crystal surface emitting lasers (PCSELS; Hirose et al. 2014; Miyai et al. 2006; Imada et al. 1999; Ohnishi et al. 2004; Sakai et al. 2005). In the PCSEL, lasing occurs through Bragg diffraction and in-plane feedback (Kurosaka et al. 2008) brought about by the periodic variation in refractive index of the photonic crystal (PC). PCSELS have been shown to give single mode emission over a large area (Hirose et al. 2014; Miyai et al. 2006; Imada et al. 1999; Ohnishi et al. 2004; Sakai et al. 2005), high power (Hirose et al. 2014), low divergence (Imada et al. 1999; Ohnishi et al. 2004), control of beam shape and polarisation (Kurosaka et al. 2008; Noda et al. 2001) and beam steering (Kurosaka et al. 2010). Typically PCSELS contain voids and are realised through wafer fusion (Noda et al. 2001; Imada et al. 1999) or through epitaxial regrowth of voids (Hirose et al. 2014). PCSELS offer some advantages over Fabry P erot (FP), distributed feedback (DFB) and vertical cavity surface emitting lasers. In particular, they promise high brightness (Hirose et al. 2014; Imada et al. 1999) and power scaling whilst maintaining circular shape of beam and low divergence angles. Many of these properties are desirable in a wide range of applications, for example low divergence beams are desirable for working towards lens-less laser modules.

Within a photonic crystal laser, light traveling within in-plane will undergo multiple scattering events. Figure 1 shows a schematic of scattered light waves in a photonic crystal consisting of circular pillars on a square lattice, showing in plane and out of plane scattering. Light is scattered backward and forward,  $\pm 90^\circ$  and out of plane. The four scattering directions are coupled and a 2D standing wave is formed. Light scattered out of plane becomes the lasing light emitted normal to the surface. The in-plane scattering of coupled light gives rise to lasing from the entire PCSEL surface and enables lasing from a large area. This leads to high power and low divergence (a requirement for high brightness).

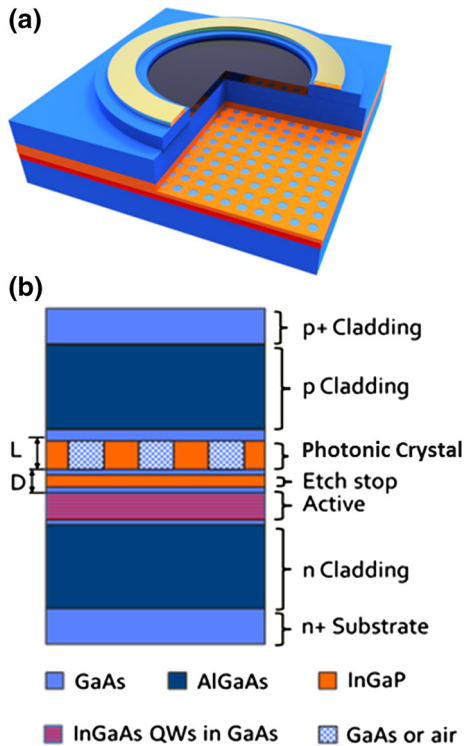
Williams et al. (2012a, b) demonstrated the first all-semiconductor PCSEL based on epitaxial regrowth, which incorporates an all-semiconductor PC rather than a void containing PC. These devices were modelled as a 1D waveguide and were shown to have a higher mode overlap and coupling than similar void containing structures. This result was subsequently confirmed by Taylor et al. (2013).

Figure 2a shows a 3D schematic of a PCSEL structure, whilst Fig. 2b shows the layer structure of the same device. PC layer thickness ( $L$ ) and the separation between active elements and the PC layer ( $D$ ) are highlighted. The structure considered is similar to Williams et al. (2012a, b) and consists of (from bottom to top) a n-type AlGaAs lower

**Fig. 1** Schematic of PCSEL scattering directions



**Fig. 2** Schematic of PCSEL 3D cross section (a) and layer structure (b)



cladding layer, a three quantum well active layer consisting of three 8 nm InGaAs quantum wells separated by 20 nm GaAs layers, an etch stop layer, the photonic crystal region of 150 nm which is InGaP/GaAs for the all-semiconductor case and InGaP/air for the void containing case, a p-type AlGaAs cladding layer and finally a highly doped p-type GaAs layer. Table 1 shows the layer structure and refractive indices of the GaAs based PCSEL considered in this paper.

Much of the work in modelling PCs has concentrated on the design of photonic crystal shape and lattice geometry (Sakai et al. 2006; Plihal and Maradudin 1991; Nielsen et al. 1999; Yokoyama and Noda 2003; Kurosaka et al. 2009), to date the effect of the waveguide design on PCSEL performance has not been comprehensively studied. This may in part be due to difficulties in engineering waveguides which contain the low average mode index associated with void containing PCSELS (Taylor et al. 2013).

Semiconductor lasers are ubiquitous. Short wavelengths are desirable for many applications including 405 nm for optical data storage (Mitsubishi 1997), laser lighting, and biomedical applications (Brezinski 2006). 1.3 and 1.55 μm lasers are the workhorses of optical communications and optical gyroscopes (Lefevre 2014) because of the dispersion and absorption properties of silica fibre (Mitschke 2009). Infra-red (IR) quantum cascade lasers (QCLs) are attractive for a range of applications including security applications such as target illumination and counter measures, and for high sensitivity gas sensing (Werlea et al. 2001).

In this paper we consider an effective refractive index model for both all semiconductor (Williams et al. 2012a) and identical void containing designs. For this basic structure emitting at ≈ 980 nm, we initially consider the effect of PC radius on the confinement of

**Table 1** Epitaxial layer structure of device considered

Material	Thickness (nm)	Refractive index
$\text{Al}_{0.4}\text{Ga}_{0.6}\text{As}$	3000	3.31
GaAs	T	3.521
GaAs	80	3.521
$\text{In}_{0.48}\text{Ga}_{0.52}\text{P}/\text{GaAs}$ or $\text{In}_{0.48}\text{Ga}_{0.52}\text{P}/\text{void}$	L	$n_{\text{av}}$
GaAs	20	3.521
$\text{In}_{0.48}\text{Ga}_{0.52}\text{P}$	40	3.143
GaAs	20	3.521
$\text{In}_{0.2}\text{Ga}_{0.8}\text{As}$	8	3.736
GaAs	20	3.521
$\text{In}_{0.2}\text{Ga}_{0.8}\text{As}$	8	3.736
GaAs	20	3.521
$\text{In}_{0.2}\text{Ga}_{0.8}\text{As}$	8	3.736
GaAs	30	3.521
$\text{Al}_{0.4}\text{Ga}_{0.6}\text{As}$	3000	3.31

the optical mode and overlap with the PC and active elements. In conventional laser design the mode overlap with the active region is considered as a key parameter, particularly in reducing threshold gain. For a PCSEL the coupling coefficient of the PC is a critical factor in achieving well separated (in wavelength) vertically emitting modes and in obtaining high power output per unit area. We find that the highest coupling to the grating occurs when the separation between the PC and active elements is small and in these regimes the overlap with the active is also maximised. As such this paper focuses on optimising the coupling coefficient of the structure alone.

The low effective refractive index of the void containing PC is highlighted as a key issue in PCSEL design. We go on to explore the use of an additional wave-guiding layer (ballast layer) above the PCSEL, and the use of a PC above and below the active element. Trends are assessed, and comparisons are made between all-semiconductor and void-containing PCSELS. General guidelines are deduced for PCSEL waveguide design. We show that the inclusion of a ballast layer increases the PC coupling for both all-semiconductor and void containing structures but that all-semiconductor PCSELS still have a higher coupling. The double decker structure is shown to increase the PC coupling and is the first structure in this study to give a higher coupling for void containing PCSELS than for all-semiconductor PCSELS, however we highlight the complexity in manufacturing such a device.

We go on to consider PCSEL designs for different material systems and wavelengths. The wavelengths considered are 405 nm (Kawashima et al. 2010) based in GaN, 1.3  $\mu\text{m}$  (Imada et al. 1999) based on InP and 10  $\mu\text{m}$  based on InP. We show that for standard edge-emitting designs for these key laser wavelength, PCSEL structures may be readily realised. We show how for all these designs, utilising a range of materials, and spanning a large spectral range, high PC coupling coefficients are obtained and thus it is possible for PCSELS to cover a full range of Laser applications.

## 2 Definitions

Figure 3 shows a plan-view schematic of a photonic crystal where, key parameters are defined. In this paper, as in Taylor et al. (2013): the base material B shall be referred to as the background material, material A shall be referred to as the atom. The PC period,  $a$ , is consistent across the whole PC,  $r$  is the atom radius and is constant for each atom. The atom radius is expressed as a fraction of the period. All photonic crystals considered consist of a circular atom on a square lattice where the materials are either InGaP/GaAs or InGaP/air, and shall be referred to as all-semiconductor or void containing, respectively.

## 3 Structure design

### 3.1 Introduction

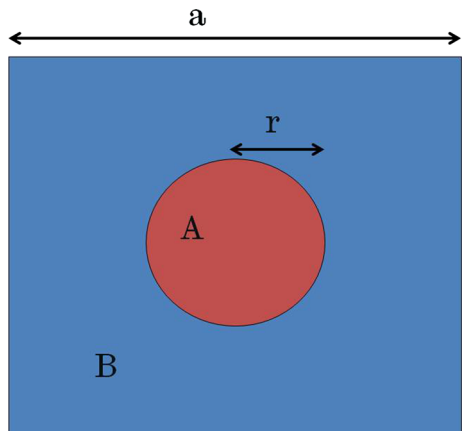
In this section the structure from Williams et al. (2012a) is modelled to confirm that results are similar. The structure is modified to include an additional GaAs waveguide layer (termed ballast layer) and to include an additional PC layer (termed double decker). These structures are modelled in the same way and compared to the original structure.

### 3.2 Basic models

There are two main methods of calculating electromagnetic fields and their characteristics of PCSELS: finite-difference time domain (FDTD) method and models relying on coupled mode theory. FDTD method is time and computer memory consuming. Models based on coupled mode theory were initially developed for modelling of distributed feedback (DFB) lasers. These models are less demanding and in recent years they have been successfully applied to PCSELS (Sakai et al. 2006).

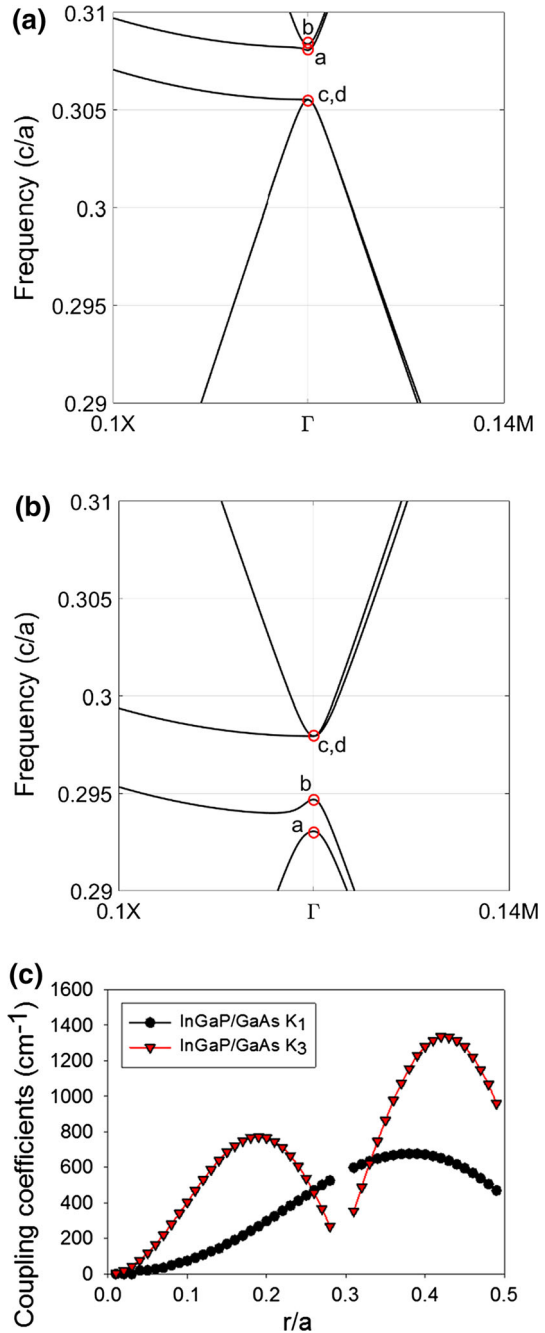
One of parameters coupled mode theory operates with is the coupling coefficient,  $K$ . The coefficient describes the feedback strength of a grating in DFB lasers and similarly of a PC in PCSELS. To keep the feedback high, one wants to make  $K$  high. The  $K$  provided by a PC with a square lattice has been derived and its relation with frequencies of bands has been established in (Sakai et al. 2006). In this work, we use band frequencies to estimate the coupling coefficient of the PCSEL rather than PC.

**Fig. 3** Schematic of a photonic crystal, indicating nomenclature used for atom and background material (A and B respectively), atom radius ( $r$ ) and unit cell size ( $a$ )



This model has been shown to be successful in the past and its implementation is relatively simple. Initially the band structure for a range of  $r/a$  ratios is modelled using MIT photonic bands (MPB) (Johnson and Joannopoulos 2001). Figure 4a, b show two such

**Fig. 4** **a** Photonic band diagram showing bands a, b, c and d of all-semiconductor InGaP/GaAs PC with  $r/a = 0.2$ ; **b**  $r/a = 0.4$ . Both diagrams calculated near  $\Gamma$  point. **c** Modelled coupling  $K_1$  (black) and  $K_3$  (red) for radius from  $0.01a$  to  $0.5a$ . (Color figure online)



band diagrams at  $r/a$  ratios of 0.2 and 0.4, respectively. Four bands, namely a, b, c, and d have been identified at  $\Gamma$  point in the band diagram and their normalized frequencies have been measured from these diagrams. These normalized frequencies in turn have been used to compute  $\omega_{a,b,c,d}$  and the coupling coefficients analytically from Eqs. (1) and (2) (Sakai et al. 2006), where  $K_1$  is the in-plane coupling coefficient,  $K_3$  is orthogonal coupling,  $n_{av}$  is the average index of the PC and  $\beta_0 = 2\pi/a$ .

$$\omega_{c,d} = \frac{c}{n_{av}} (\beta_0 + K_3) \left( 1 - \frac{4K_1^2}{\beta_0^2 - K_3^2} \right). \tag{1}$$

$$\omega_b = \frac{c}{n_{av}} (\beta_0 - K_3). \tag{2}$$

$$\omega_a = \frac{c}{n_{av}} (\beta_0 - K_3) \left( 1 - \frac{8K_1^2}{\beta_0^2 - K_3^2} \right). \tag{3}$$

Figure 4c shows modelled coupling coefficients  $K_1$  (black) and  $K_3$  (red), for a PC consisting of InGaP/GaAs on a square lattice with a circular lattice, for a range of atom radii from 0 to 0.45  $r/a$ . The dependence of  $K_3$  has two local maxima at  $r/a$  of 0.2 and 0.4, they correspond to band diagrams with largest frequency differences between bands shown in Fig. 4a, b. At around  $r/a = 0.3$ , bands cross and deduction of coupling coefficients becomes difficult.

For  $K_1$ , the coupling coefficient generally increases as atom radius increases until a radius of 0.4, when the coupling decreases again. For  $K_3$ , the coupling coefficient has a double peak at  $r = 0.15a$  and  $r = 0.4a$ . The coupling coefficients are not plotted at a radius of  $\sim 0.3a$  as this corresponds to a change in character of the band structure and the assignment bands is complicated as the bands cross (Taylor et al. 2013). The dual peak nature of  $K_3$  has been identified previously (Yokoyama and Noda 2005), and is similar to results shown in Taylor et al. (2013). We note that this model may be limited in its viability because it assumes that the PC is infinite. It is therefore only truly valid in the case where the electric field intensity does not vary across the thickness of the PC layer, in the case of a comparatively thick layer with a bound mode this is not necessarily true.

Figure 5 shows the modelled mode profile of the PCSEL overlaid on a schematic of the structure described in Sect. 1, where in this case the structure is modelled as a one dimensional waveguide using FIMMWAVE (<http://www.photond.com/products/fimmwave.htm>). Figures a–c show the mode profile of an all-semiconductor PCSEL (dashed line) and void containing PCSEL (solid line) where the atom radius of the PC is 0.1a, 0.3a and 0.45a respectively. The mode of the void containing structure are distorted away from the PC, which is attributed to the low refractive index of the PC in the void containing case, which results in low mode overlap with the PC.

From the mode profile the coupling coefficient is calculated using  $K = \Gamma_{PC} \frac{2 \times \Delta n}{\lambda}$  (where  $\Gamma_{PC}$  is mode overlap with the PC,  $\Delta n$  is the refractive index contrast and  $\lambda$  is vacuum wavelength). Figure 6 shows coupling as distance between active elements and PC region is increased for all-semiconductor and void containing structures. As  $D$  is increased the coupling coefficient decreases, as the PC has ever decreasing interaction with the in-plane waveguided mode. For the full range of  $D$  considered, the all-semiconductor PCSEL has a higher coupling coefficient than the void-containing counterpart. As with the previous

**Fig. 5** Modelled mode profile of PCSEL structure overlaid on structure schematic for atom radius of **a** 0.1a, **b** 0.3a and **c** 0.45a

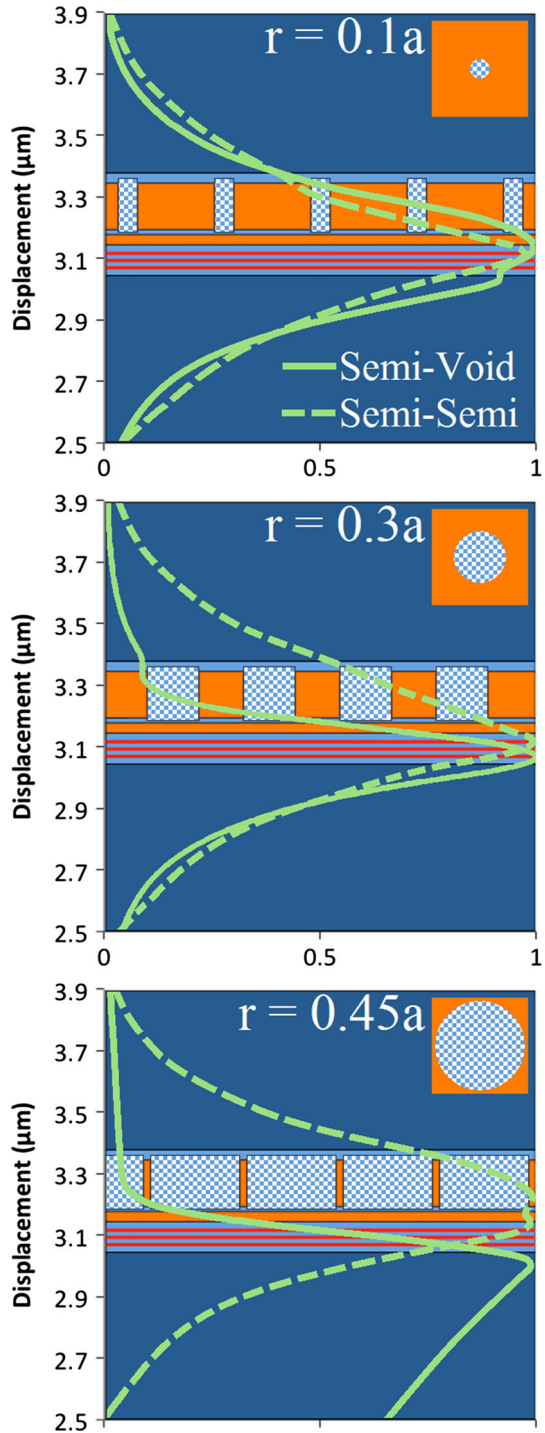
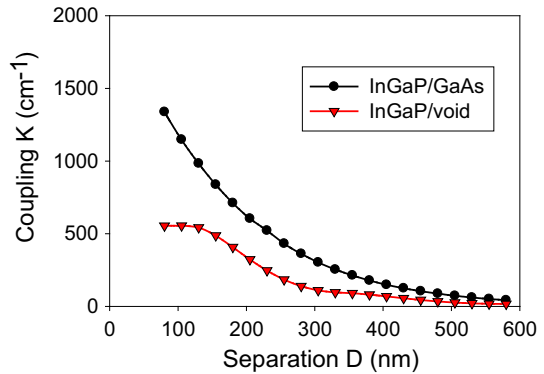




**Fig. 6** Coupling variation for separation thickness  $D$  from 40 to 600 nm for InGaP/GaAs (*black*) and InGaP/void (*red*). (Color figure online)



example this model also has limitations as it considers only the waveguide and does not consider PC effects such as feedback and scattering.

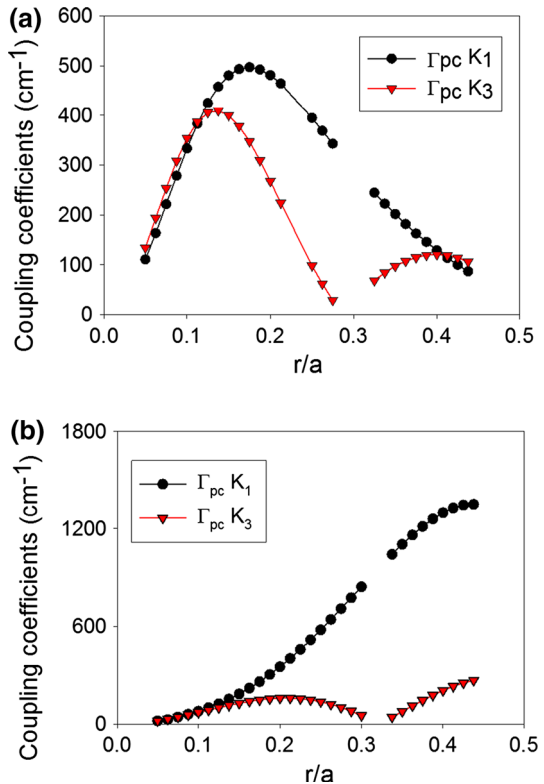
### 3.3 Basic structure

In this section we combine the two models mentioned previously to consider the effect of both the PC and the waveguide on the coupling coefficient. Here the coupling coefficient calculated for the PC from the band-structure and Eqs. (1) and (2) is multiplied by the confinement factor. This method shall be used to calculate all subsequent coupling coefficients. Figure 7 shows the coupling coefficient  $K_1$  (black) and  $K_3$  (red) for (a) void containing and (b) all-semiconductor PCSEL, for a range of atom radius from 0.05 to 0.45a. For the void containing structure,  $K_3$  has two peaks one at 0.15a and one at 0.4a, while  $K_1$  has a global peak at 0.175a. The all semiconductor PCSEL again has two peaks for  $K_3$ , at 0.2a and 0.45a, while the  $K_1$  has a peak at 0.45a. The maximum peak in  $K_1$  is  $500 \text{ cm}^{-1}$  for the void containing structure and  $1300 \text{ cm}^{-1}$  for the all-semiconductor case. In the case of Fig. 6b mode overlap does not change significantly as  $r/a$  ratio is increased. In the case of the void containing PCSEL (Fig. 7a), when  $r/a$  is high, the low  $n_{av}$  pushes the mode away which dominates, giving a relatively low coupling coefficient. For low  $r/a$  void containing PCSELS have higher coupling coefficients, while all semiconductor PCSELS have a higher coupling at large  $r/a$ .

It is expected that the thickness of the PC layer will have an effect on the coupling coefficient of a PCSEL due to the change in modal structure and overlap integral. For the moment we ignore the need for the PC to be of specific thickness to ensure constructive interference in the far-field. Figure 8 shows the coupling coefficient  $K_1$  of (a) void containing and (b) all-semiconductor PCSEL where the atom radius is increased from 0.05 to 0.45a, for PC thickness ( $L$ ) of 50 nm (black), 150 nm (red), 300 nm (green) and 400 nm (orange). For the void containing structure the peak coupling occurs at either 0.15a or 0.25a, and coupling decreases as PC thickness increases, this is due to the low refractive index of the PC layer further distorting the mode away from the PC layer. The all-semiconductor structure has a peak at 0.4a, increasing PC layer thickness ( $L$ ) increases the coupling, this can be attributed to the PC layer having increased volume for the mode to couple to.

Figure 9 shows the same as Fig. 7 for coupling coefficient  $K_1$ , in this case the void containing structure has two peaks at 0.125a and 0.4a, the peak coupling occurs for PC layer thickness of 150 nm. The all-semiconductor structure has a local peak in coupling at

**Fig. 7** **a** Coupling coefficient  $K_1$  (black) and  $K_3$  (red) for void containing PCSEL. **b** Coupling coefficient  $K_1$  (black) and  $K_3$  (red) for all-semiconductor PCSEL. (Color figure online)



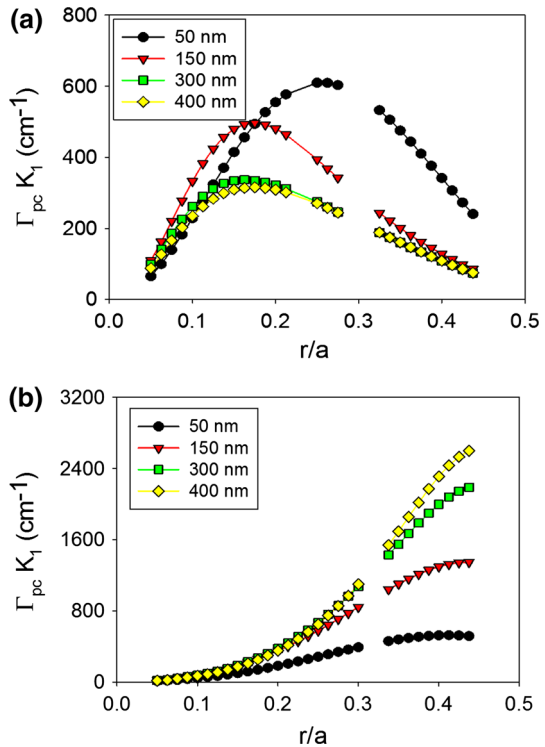
0.2a and a global peak in coupling at 0.45a, as the PC thickness increases the coupling also increases.

In general, for this structure, we find that an increase in PC layer thickness has a monotonical improvement at an  $r/a$  of 0.4, this is enabled by the  $n_{\text{av}}$  of the PC layer being similar to the refractive index of the waveguide. In the void containing PC case, a thicker PC layer has detrimental effects due to the low  $n_{\text{av}}$ . Our observed maxima in coupling at  $r/a = 0.2$  for 150 nm PC thickness, is in agreement with observed values in the literature.

### 3.4 Ballast layer structure

As discussed previously, PCSEL structures containing voids have lower coupling of the optical mode to the photonic crystal as compared to their all-semiconductor counterparts. This is attributed to the low refractive index of the PC layer “pushing” the optical mode away from the PC region. In order to address this, we consider a structure which includes an additional p-type GaAs waveguide region above the PC region (of thickness  $T$  in Table 1). This additional layer is referred to as the ballast layer. This layer is intended to “pull” the mode higher in the structure and increase mode overlap with the PC region. Figure 10 illustrates this by plotting the modelled mode profile of a void containing PCSEL with a ballast layer (dashed line) and without a ballast layer (solid line), for atom radius 0.1a (a), 0.3a (b) and 0.45a (c). The mode overlap with the PC is increased for

**Fig. 8** Coupling coefficient  $K_1$  of **a** void containing and **b** all-semiconductor PCSEL for atom radius from 0.05 to 0.45a, for PC thickness (L) of 50 nm (black), 150 nm (red), 300 nm (green) and 400 nm (orange). (Color figure online)



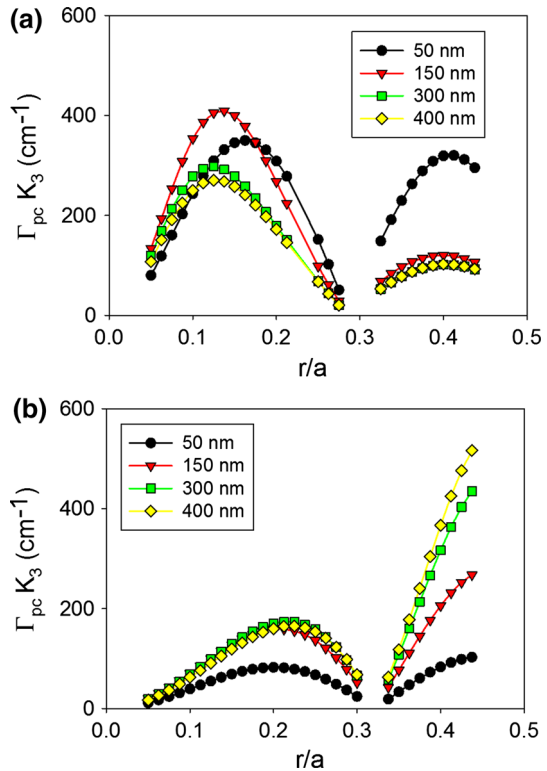
$r = 0.1a$  and  $r = 0.3a$ . For  $r = 0.1a$  the mode peak is entirely shifted to overlap with the PC layer, this has the side effect of reducing the mode overlap with the quantum wells. At  $r = 0.3a$  a second peak in the mode profile has appeared within the ballast layer, giving an increased mode overlap with the PC layer. For  $r = 0.45a$  the inclusion of the ballast layer has little effect on the mode profile, this is due to the very low average refractive index of the PC layer in this case.

Figure 11 shows the coupling coefficient  $K_1$  as atom radius increases from 0.05a to 0.45a, for a void containing PCSEL (a) and an all-semiconductor PCSEL (b), for ballast layer thicknesses from  $T = 0-500$  nm. For the void containing PCSEL peak coupling occurs at  $r = 0.2a$ . As ballast layer thickness ( $T$ ) increases the coupling increases to a maximum of  $\sim 800 \text{ cm}^{-1}$  at  $T = 100$  nm, as  $T$  is increased beyond 100 nm coupling decreases. For the all-semiconductor PCSEL the ballast layer reduces the coupling coefficient, and as ballast layer thickness is increased the coupling decreases.

Figure 12 shows the same plot as Fig. 10 for coupling coefficient  $K_3$ , in both cases a double peak is observed and coupling is increased as  $T$  is increased from 0 to 100 nm then decreases as the ballast layer thickness is increased further. For the void containing PCSEL peaks occur at  $r = 0.15a$  and  $r = 0.4a$ , while for the all-semiconductor PCSEL peaks occur at  $0.2a$  and  $0.45a$ .

The ballast layer has been shown to distort the mode profile of the PCSEL, for both the all-semiconductor and the void containing PCSEL a ballast layer of 100 nm gives the highest coupling. A ballast layer of suitable thickness has a significantly advantageous

**Fig. 9** Coupling coefficient  $K_3$  of **a** void containing and **b** all-semiconductor PCSEL for atom radius from 0.05 to 0.45a, for PC thickness (L) of 50 nm (black), 150 nm (red), 300 nm (green) and 400 nm (orange). (Color figure online)



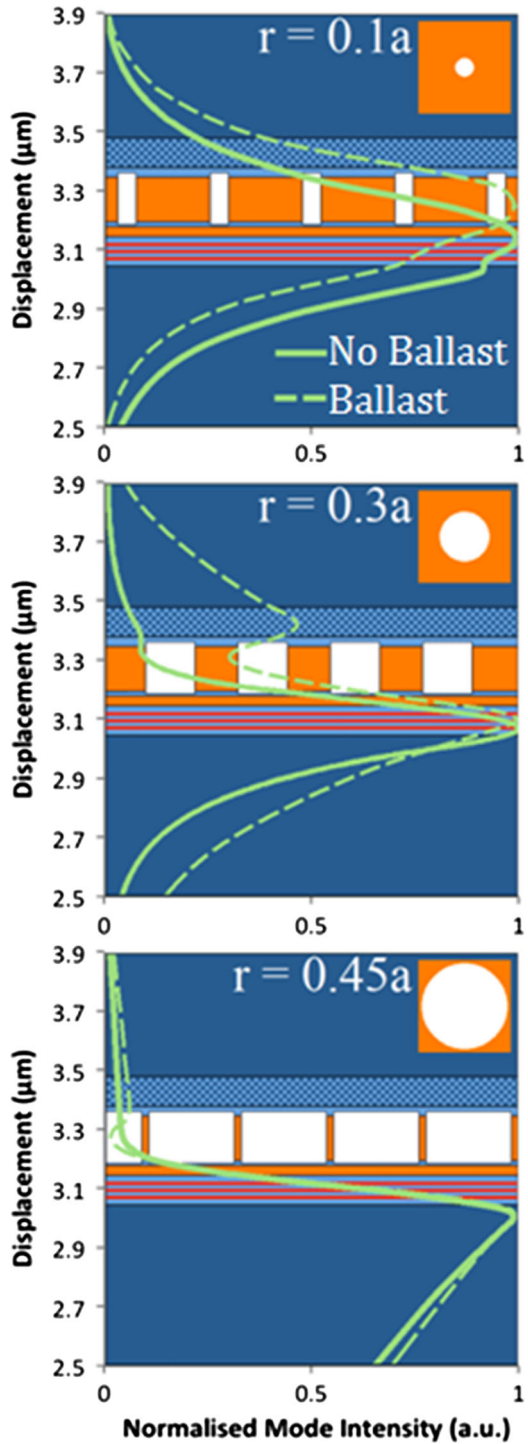
effect for void containing PCSELs at an  $r/a$  of 0.2. For all-semiconductor PCSEL, a marginal effect is observed with no detriment to the structural design. This bodes well for a one step epitaxial process in Williams et al. (2012a) where  $T$  may vary between runs. It is of note that the all semiconductor PCSEL has a significantly higher global maximum in coupling coefficient.

### 3.5 Double decker

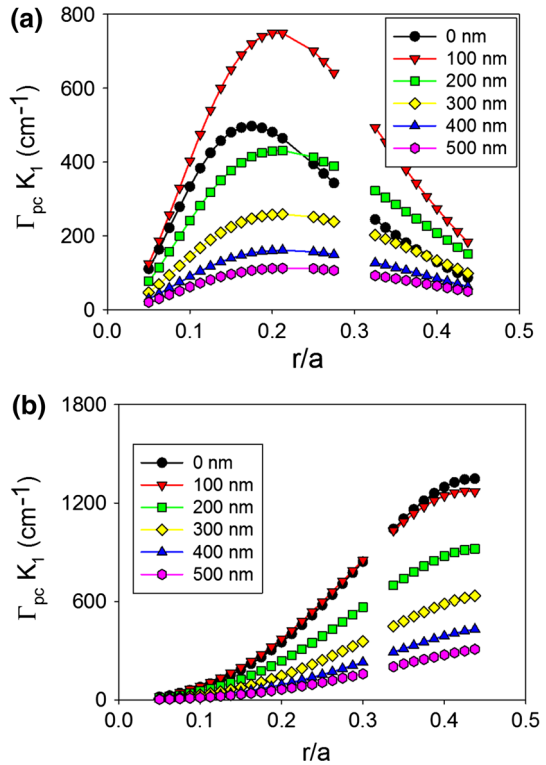
The final structure considered in this section, consists of two PC regions located above and below the active region, first proposed by Kurosaka et al. (2008) The intention with this structure is that by having 2 PC regions the coupling will be increased by virtue of there being more overlap of the confined mode with the PC and the symmetry of the structure should allow the realisation of strongly bound modes for void containing PCSELs to be combined with the high index contrast that they offer. Figure 13 shows a schematic of a double decker PCSEL, where the structure consists (from bottom to top) a n-type cladding layer, an etch stop layer, photonic crystal region, a three quantum well active layer, an etch stop layer, photonic crystal region, a p-type cladding layer and finally a highly doped p-type layer. Table 2 shows the layer structure of a double decker PCSEL.

Figure 14 shows the modelled mode profile overlaid on schematic of the structure, of an all-semiconductor (dashed) and void (solid) double decker PCSEL, for atom radius 0.1a (a), 0.3a (b) and 0.45a (c). In each case the mode is centred on the active region, for the all-semiconductor PCSEL, as atom radius is increased the mode is less tightly bound and mode

**Fig. 10** Modelled mode profile of a void containing PCSEL with a ballast layer (*dashed line*) and without a ballast layer (*solid line*), for atom radius  $0.1a$  (a),  $0.3a$  (b) and  $0.45a$  (c)



**Fig. 11** Coupling coefficient  $K_1$  as atom radius increases from  $0.05a$  to  $0.45a$ , for a void containing PCSEL (a) and an all-semiconductor PCSEL (b), for a ballast layer thickness of  $0$ – $500$  nm



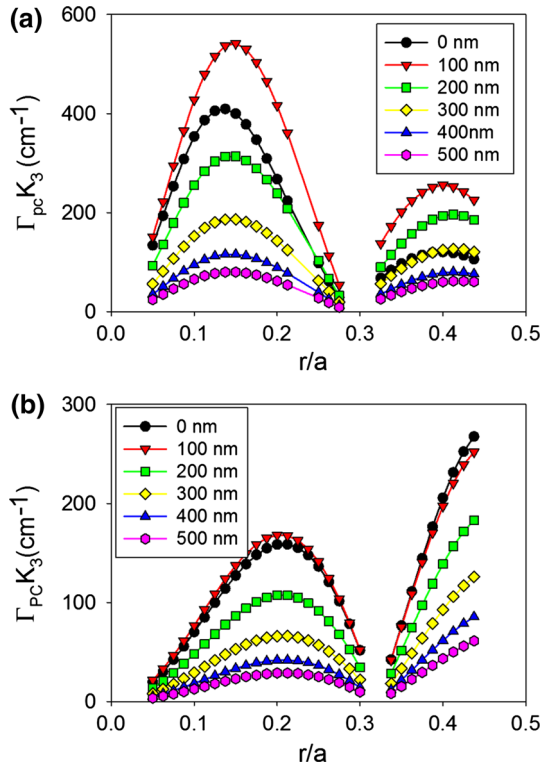
of the mode leaks into the cladding layers. For the void containing PCSEL the mode is more tightly bound as the atom radius increases due to the symmetry of these low refractive index waveguiding layers.

Figure 15 shows the coupling coefficient  $K_1$  as atom radius increases from  $0.05a$  to  $0.45a$ , for a void containing (a) and an all-semiconductor (b) double decker PCSEL, for separation distance ( $L$ ) from  $0$  to  $200$  nm. For the void containing PCSEL with separation of  $0$  and  $50$  nm the coupling is  $0$  above  $0.2a$  and  $0.3a$ , respectively, because there is no bound mode in this case, for separation distance  $>50$  nm coupling is optimum at  $r = 0.25a$  and decreases as separation decreases. For the all-semiconductor PCSEL the coupling is greatest at  $r = 0.4a$ , as separation ( $L$ ) increases the coupling decreases.

Figure 16 shows the same plot as Fig. 14 for coupling coefficient  $K_3$ , in both cases a double peak is observed and coupling is decreased as  $L$  is increased from  $0$  to  $200$  nm. For the void containing PCSEL peaks occur at  $r = 0.15a$  and  $r = 0.4a$ , while for the all-semiconductor PCSEL peaks occur at  $0.2a$  and  $0.45a$ . The double decker void containing PCSEL has peak coupling ( $K_3$ ) of  $1000 \text{ cm}^{-1}$  at  $r = 0.15a$ , this is a two fold increase in coupling compared with the original structure.

It is worth noting that fabricating a double decker PCSEL with wafer fusion would leave fusion interfaces within nm of the active region, which may result in defect states within the junction region of the structure. This may have significant impact on performance, reliability, and repeatability. Furthermore, the two PC layers would need to be “perfectly” aligned which would require  $\sim$  nm precision over the  $2$ – $6$  inch wafer which would also be

**Fig. 12** Coupling coefficient  $K_3$  as atom radius increases from  $0.05a$  to  $0.45a$ , for a void containing PCSEL (a) and an all-semiconductor PCSEL (b), for a ballast layer thickness of 0–500 nm



**Fig. 13** Schematic of a double decker PCSEL

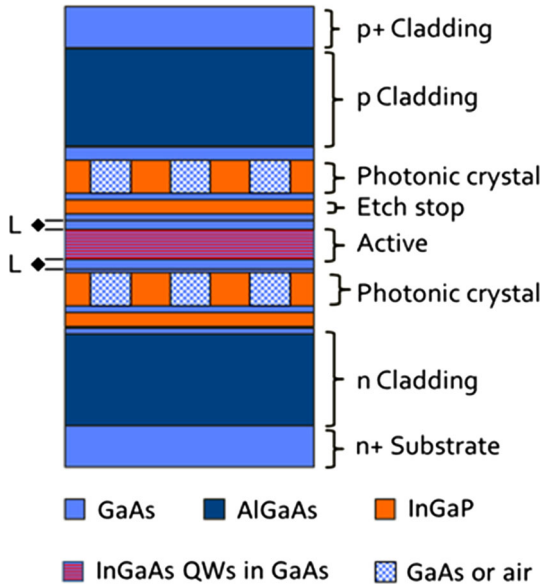


**Table 2** Layer structure of double decker structure

Material	Thickness (nm)	Refractive index
Al <sub>0.4</sub> Ga <sub>0.6</sub> As	3000	3.31
GaAs	T	3.521
GaAs	80	3.521
In <sub>0.48</sub> Ga <sub>0.52</sub> P/GaAs or In <sub>0.48</sub> Ga <sub>0.52</sub> P/void	150	n <sub>av</sub>
GaAs	20 + L	3.521
In <sub>0.48</sub> Ga <sub>0.52</sub> P	40	3.143
GaAs	20	3.521
In <sub>0.2</sub> Ga <sub>0.8</sub> As	8	3.736
GaAs	20	3.521
In <sub>0.2</sub> Ga <sub>0.8</sub> As	8	3.736
GaAs	20	3.521
In <sub>0.2</sub> Ga <sub>0.8</sub> As	8	3.736
GaAs	30 + L	3.521
In <sub>0.48</sub> Ga <sub>0.52</sub> P/GaAs or In <sub>0.48</sub> Ga <sub>0.52</sub> P/void	150	n <sub>av</sub>
Al <sub>0.4</sub> Ga <sub>0.6</sub> As	3000	3.31

challenging. Fabricating a double decker PCSEL by epitaxial regrowth would require multiple re-growths, though alignment may be less of an issue for regrown PCSELS because a feature could be etched into layer 1 to act as an alignment marker during the patterning of the PC layers. Nevertheless, “perfect” alignment would be a major technical challenge, and the double-decker PCSEL poses a number of challenges in terms of practical realisation in a robust manufacturable manner. By contrast to the previous cases, optimal void containing structures and all-semiconductor structures have similar characteristics. The key difference being the ratio of  $K_1$  to  $K_3$ , the effect of comparative ratio has been discussed elsewhere (Taylor et al. 2013).

### 3.6 Summary

In this Section 980 nm PCSELS based on GaAs were simulated by combining waveguide and band structure modelling. We find that  $n_{av}$  plays an important role in waveguide engineering. For an all-semiconductor PCSEL the photonic crystal has a  $n_{av}$  similar to the rest of the waveguide, allowing flexibility in waveguide design. A large  $r/a$  ratio can be achieved while a strong mode overlap (and hence high  $K$ ) can be maintained. For void containing structures there is a tendency for optimal coupling to occur at radius to be at  $\sim 0.2 r/a$ , this is in contrast to the all-semiconductor PCSEL where optimal coupling occurs at  $\sim 0.4 r/a$ . The addition of a ballast layer increases the peak coupling values for both all-semiconductor and void containing PCSELS, with the largest effect for a ballast layer thickness of 100 nm. The inclusion of a second PC layer (double decker PCSEL) leads to an increase in coupling coefficients, particularly with void containing structures where the low average refractive index of the PC layer strongly confines the mode between the PC layers within the active region. However, it is worth noting that the realisation of a double decker structure poses significant fabrication issues.



**Fig. 14** Modelled mode profile overlaid on schematic of the structure, of an all-semiconductor (*dashed*) and void (*solid*) double decker PCSEL, for atom radius 0.1a (**a**), 0.3a (**b**) and 0.45a (**c**)

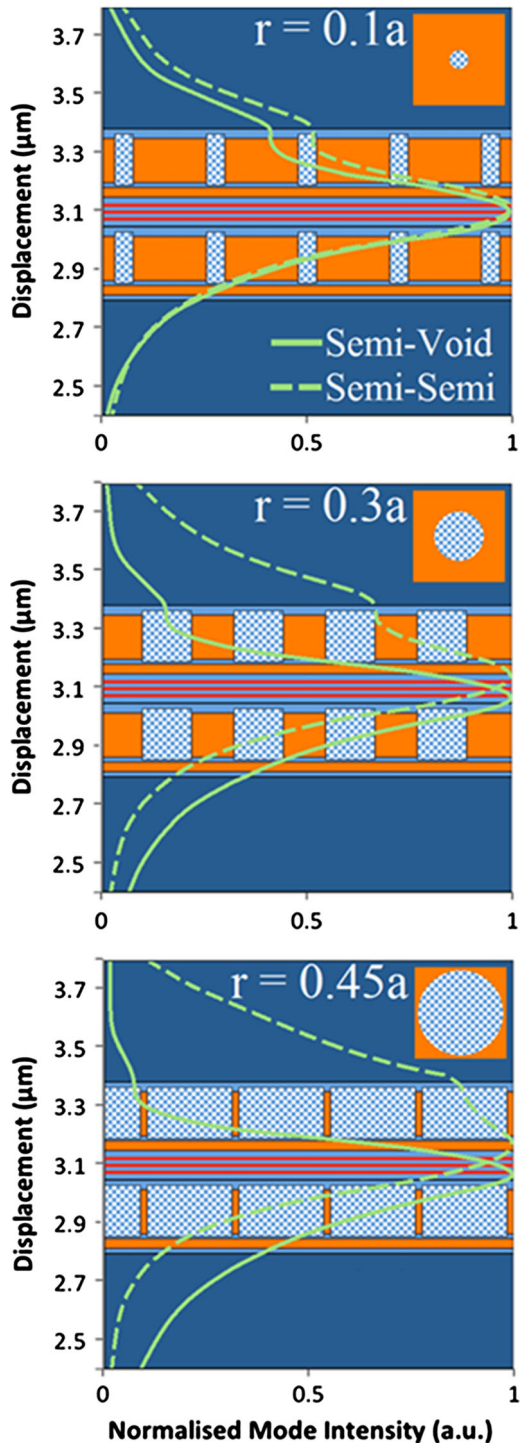
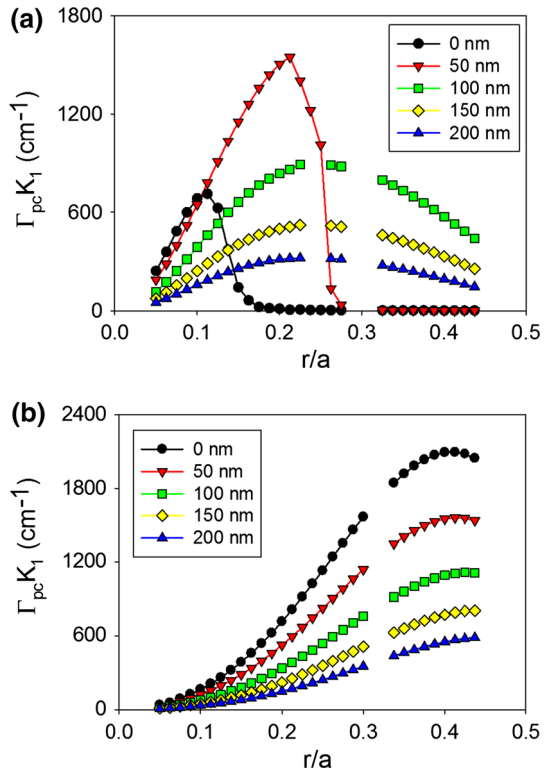


**Fig. 15** Coupling coefficient  $K_1$  for atom radius increases from  $0.05a$  to  $0.45a$ , for **a** void containing and **b** all-semiconductor double decker PCSEL, for separation distance ( $L$ ) from 0 to 200 nm



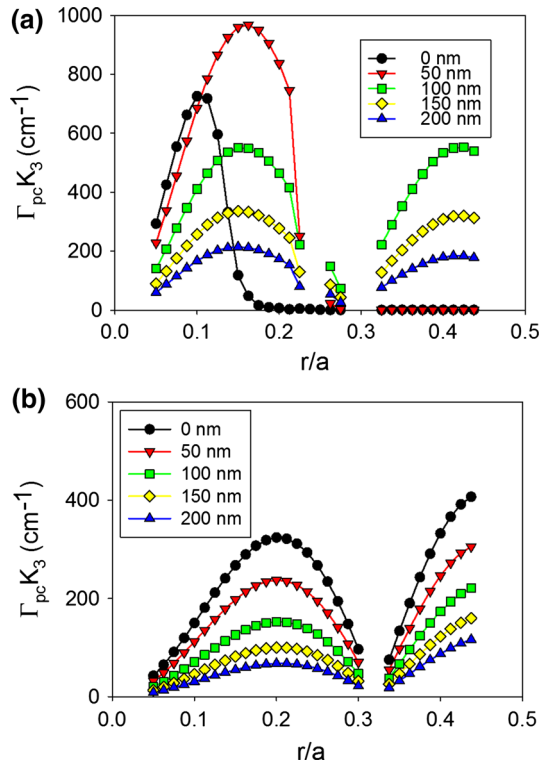
## 4 Material design

### 4.1 Introduction

In this section we consider PCSEL designs for different material systems and wavelengths. The wavelengths considered are 405 nm (AlInGaN) (Kawashima et al. 2010), 1.3  $\mu\text{m}$  (InGaAsP) (Noda et al. 2001) and 10  $\mu\text{m}$  (AlInGaAsP QCL). Each structure is once more modelled as a 1D waveguide where the PC region is considered as a layer with a refractive index determined by an average of the PC constituents. The coupling coefficient is calculated for various separation thickness variations and for various photonic crystal thicknesses. Three PC thicknesses are considered, H, 2H and 3H where H is  $\lambda/2n_{av}$  (where  $\lambda$  is the vacuum wavelength and  $n_{av}$  is the average refractive index in the PC).

All-semiconductor PCSEL have primarily operated at 980 nm and been based on GaAs overgrowth, there has been little work on all-semiconductor PCSEL operating at different wavelengths or other materials. Previous work on a range of materials systems in the literature (Noda et al. 2001; Kawashima et al. 2010) has revolved around void/semiconductor PCSELs with comparatively small atom radius, due to the design considerations highlighted in the previous sections. However, here we wish to explore the possibilities of utilizing high mode overlap (and hence high coupling coefficient) all-semiconductor designs. As a consequence, in all cases a 50% fill factor is considered, this is taken from Sect. 2 and Taylor et al. where they find 50% fill to give a maximum in coupling. This allows simulation and comparison of PCSEL structures for a range of material systems.

**Fig. 16** Coupling coefficient  $K_3$  for atom radius increase from  $0.05a$  to  $0.45a$ , for **a** void containing and **b** all-semiconductor double decker PCSEL, for separation distance ( $L$ ) from 0 to 200 nm

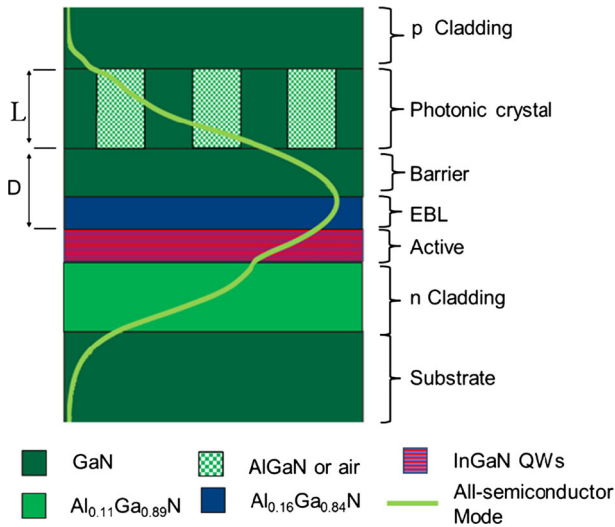


### 4.2 GaN/InGaN/AlGaIn 405 nm structure

GaN is the material of choice for short wavelength lasers  $\sim 400$  nm. This has been primarily targeted for applications in optical data storage, displays, and biomedical applications (Mitsuhashi 1997; Lefevre 2014). Incorporating a photonic crystal within a GaN laser structure would allow the aforementioned advantages of PCSELS to be realised at these wavelengths. A  $\sim 400$  nm void containing PCSEL has been realised by Kawashima et al. (2010).

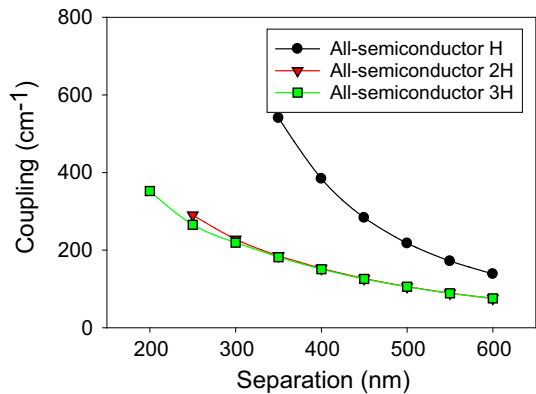
Figure 17 shows the structure of a  $\sim 400$  nm PCSEL design after the layer sequence described in Kawashima et al. (2010). The structure consists of (from bottom to top) n-type  $\text{Al}_{0.11}\text{Ga}_{0.89}\text{N}$  cladding layer, followed by an 80-nm-thick n-doped GaN layer, multiple quantum wells (MQWs), an 80-nm-thick undoped GaN layer, a 20-nm-thick p- $\text{Al}_{0.16}\text{Ga}_{0.84}\text{N}$  electron-blocking layer (EBL), a 115-nm-thick p-GaN layer, a PC layer, a 40-nm-thick p-GaN layer and a 115-nm-thick p+-GaN contact layer. The MQW active zone consists of three 2.5-nm-thick  $\text{In}_{0.09}\text{Ga}_{0.91}\text{N}$  well layers and 7.5-nm-thick GaN barrier layers. The PC region is 220 nm thick and consists of GaN/ $\text{Al}_{0.11}\text{Ga}_{0.89}\text{N}$  with a 50% fill factor. The mode profile is shown overlaid on the device structure (Fig. 17). The mode profile can be seen to significantly overlap with both the photonics crystal and active regions. Refractive indices are taken from Laws et al. (2001).

Figure 18 shows coupling as the PC separation,  $D$ , increases for GaN based 405 nm PCSEL, from Kawashima et al. (2010). The separation between the PC and the active



**Fig. 17** TE mode profile (intensity) overlaid on PCSEL structure for a 405 nm PCSEL

**Fig. 18** Coupling variation for separation width from 150 to 600 nm for GaN based 405 nm PCSEL



layer, D, is varied from 150 to 600 nm and the PC thickness is H, 2H and 3H. These thicknesses are chosen to ensure constructive interference in the far-field.

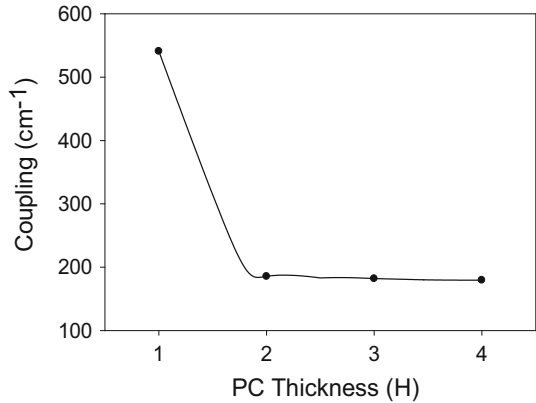
Figure 19 shows the PC coupling of a 400 nm PCSEL shown in Fig. 17, for an all-semiconductor PC where the PC thickness is increased. The coupling decreases rapidly as PC thickness increases from 1H to 2H. As thickness increases from 2H to 4H the coupling decreases steadily.

In all cases the coupling decreases as the separation thickness D increases, and as expected the coupling tends to zero for large values of D. While increasing the thickness of the PC initially reduces the coupling, further increases in the thickness gives no change to the coupling. No values of coupling are shown for thickness of H, where Separation is <350 nm as there are no modes are bound in this case.

### 4.3 InP/InGaAsP 1.3 μm structure

The absorption and dispersion characteristics of optical fibre gives two wavelength windows for optical communications at 1.55 and 1.3 μm (Mitschke 2009). Incorporating a

**Fig. 19** Coupling variation for 400 nm PCSEL for a variation in PC thickness H



photonic crystal within a InP laser structure would allow the advantages of PCSELS for optical communication applications. In particular, low divergence circular beams may allow lens-less optical communications modules to be considered. Furthermore, there are possible advantages in terms of manufacturing test and validation for surface emitters.

Figure 20 shows the structure of a 1.3 μm PCSEL which is based on a structure from Imada et al. (1999) consisting (from bottom to top): InP substrate, 1.4 μm cladding layer, 240 nm QW active layer consisting of seven 7 nm InGaAsP quantum wells with 15 nm InP barriers, a photonic crystal consisting of InGaAsP/InP with a 50% fill factor and a 1.4 μm InP cladding layer. Modelled mode profile where the mode for an all-semiconductor PC (solid line) is shown overlaid on the device structure. As observed in GaN devices the mode shows significant overlap with the PC and active layers.

**Fig. 20** TE mode profile overlaid on PCSEL structure for an all-semiconductor 1300 nm PCSEL

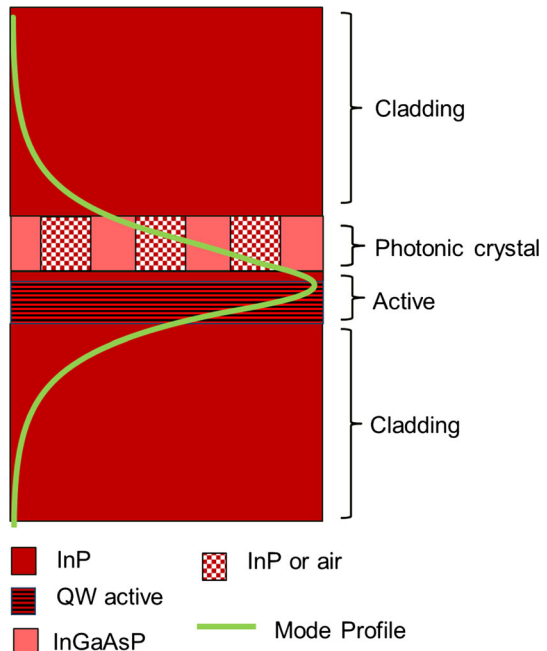


Figure 21 shows the modelled photonic crystal coupling of a 1.3  $\mu\text{m}$  PCSEL where the separation between the photonic crystal and the active region D, is varied from 0 to 600 nm where PC thickness is H, 2H and 3H. In all cases coupling approaches a maximum as separation approaches zero, as separation increases coupling decreases. Increasing the thickness of the PC layer increases the coupling, with a maximum occurring at separation of 0 nm and PC thickness of 3H, giving a maximum in coupling of  $2000\text{ cm}^{-1}$ . As expected, for large values of separation the coupling tends to zero.

Figure 22 shows the PC coupling of a 1.3  $\mu\text{m}$  PCSEL shown in Fig. 20, where the PC thickness is increased. The coupling increases as PC thickness increases from 1H to 4H and decreases as thickness is increased further, indicating that the ideal PC thickness is 3H.

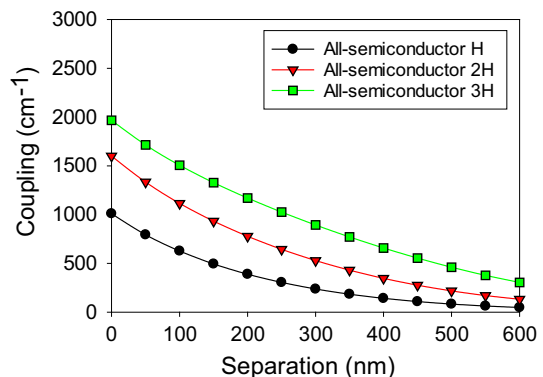
#### 4.4 InP/AlInAs/InGaAs 10 $\mu\text{m}$ structure

InP based quantum cascade lasers (QCLs) have shown promise in a range of applications including security applications such as target illumination and industrial applications such as gas sensing (Werlea et al. 2001). Here, power scaling with area and the low divergence of the PCSEL all offer significant advantages for systems applications.

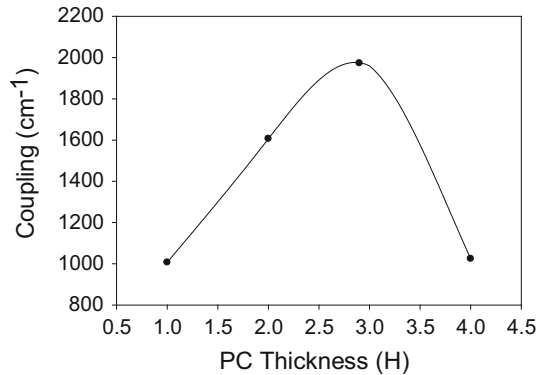
Figure 23 shows a 10  $\mu\text{m}$  quantum cascade PCSEL based on edge emitting DFB laser work by Kennedy et al. (2007). The structure consists of (from bottom to top): 2.5  $\mu\text{m}$  InP cladding layer, 270 nm InGaAs barrier layer, active region consisting of 35-stage region with the nominal layer structure of (thicknesses in Angstroms); **35/23/8/66/9/64/9/58/20/40/12/40/12/40/13/39/17/38/21/35/22/35** where bold refers to InAlAs and normal type refers to InGaAs, a photonic crystal region which consists of InP/InGaAs and has a 50% fill factor, and a 3.5  $\mu\text{m}$  InP upper cladding layer. The modelled mode profile of a 10  $\mu\text{m}$  InP QCL PCSEL where the mode profile is shown overlaid on the device structure. Refractive indices are taken from Li et al. (2001). The mode considered for this structure (unlike previous structures) is TM polarised. As in previous structures the mode is shown to have a large mode overlap with both the photonic crystal and active regions.

Figure 24 shows the photonic crystal coupling of a 10  $\mu\text{m}$  QCL PCSEL where the separation between the photonic crystal and the active region, D, is varied from 0 to 600 nm and the PC is all-semiconductor. The thickness of the photonic crystal layer is H, 2H and 3H. Coupling is observed to decrease steadily as separation increases with highest coupling of  $3000\text{ cm}^{-1}$  when separation is 0 nm and thickness is 4 H.

**Fig. 21** Coupling variation for separation width from 0 to 600 nm for 1.3  $\mu\text{m}$  PCSEL showing all-semiconductor and void containing structures



**Fig. 22** Coupling variation for all semiconductor 1.3 μm PCSEL for a variation in PC thickness H



**Fig. 23** TM mode profile overlaid on InP 10 μm PCSEL structure

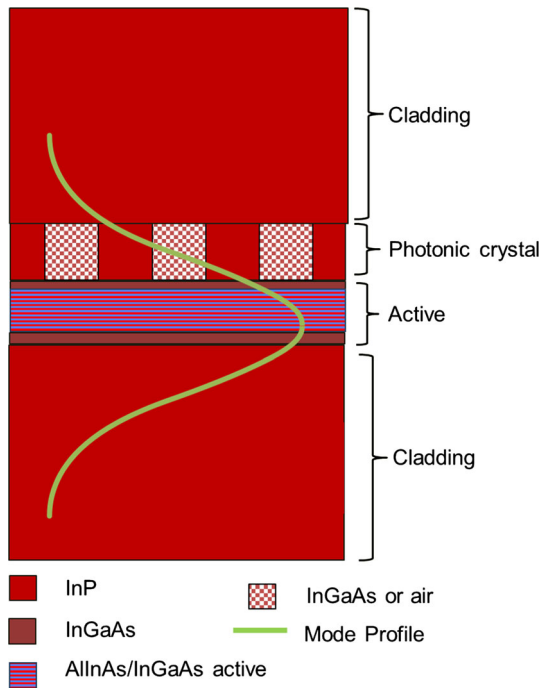
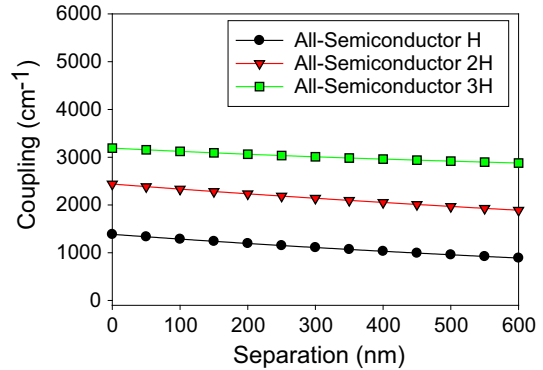


Figure 25 shows the PC coupling of the 10um InP QCL as a function of PC thickness. The coupling increases as PC thickness increases from 1H to 3H and decreases as thickness is increased further, indicating that an ideal PC thickness of 3H.

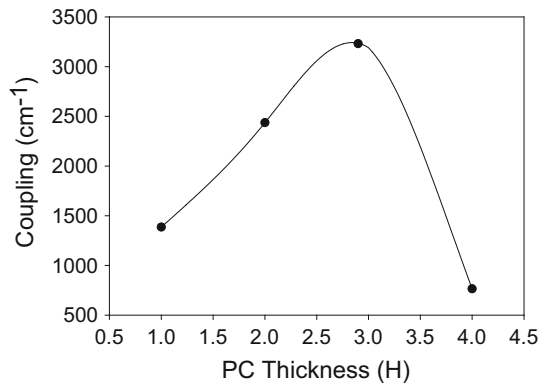
### 4.5 Summary

In this section PCSELS operating at key wavelengths were simulated by combining waveguide and band structure modelling. We find that  $n_{av}$  plays an important role in waveguide engineering. For InP structures we find that the peak photonic crystal coupling occurs at a thickness of 3H while for GaN material systems we find that a thickness of 1H

**Fig. 24** Coupling variation for separation width from 0 to 600 nm for InP based 10  $\mu\text{m}$  QCL



**Fig. 25** Coupling variation for InP based 10  $\mu\text{m}$  QCL for a variation in PC thickness H



gives the highest coupling. In all cases we find that the coupling decreases as the separation of the photonic crystal and the active layer is increased. We show that in each case it is possible to obtain strong mode overlap with both the photonic crystal and the active regions. This opens a route to realise PCSELS spanning a range of wavelengths from UV to IR.

## 5 Conclusions

In this paper we have considered three structures, a structure from Williams et al. (2012a), a ballast layer structure and a double decker structure. The coupling coefficient was calculated as a combination of the mode profile (calculated from FIMMWAVE) and the coupling calculated from the band diagram (Sakai et al. 2006), and each structure was modelled having an all-semiconductor PC and a void containing PC. In each case considered, the all-semiconductor PCSEL had higher peak coupling (both  $K_1$  and  $K_3$ ). The void containing structures all had peak coupling at atom radius  $r \sim 0.2a$ , while the all-semiconductor structures had peak coupling at  $r = 0.4a$ . By including a ballast layer within the structure the coupling was increased for ballast layer thickness  $< 100$  nm. The double decker structure gave the largest increase in the coupling, but fabricating such a structure would be problematic.



Three PCSEL structures with emission spanning the UV to mid-IR (400, 1300 nm and 10  $\mu\text{m}$ ) have been considered. To a first approximation the device design is an existing edge emitting laser structure, with a PC layer in the upper waveguide cladding. All three structures have been modelled as a 1D waveguide and PC coupling coefficients have been calculated. We show that in each case it is possible to obtain strong mode overlap with both the photonic crystal and the active regions. The realisation of PCSELS spanning a full range of key laser wavelengths will allow the many advantages of PCSELS to be implemented into a range of laser systems.

**Acknowledgements** The authors would like to acknowledge financial support provided by the EPSRC under Grant EP/K023195/1. RJET would like to acknowledge financial support provided by the EPSRC under grant EP/M506618/1 and JSPS under P15364.

**Open Access** This article is distributed under the terms of the Creative Commons Attribution 4.0 International License (<http://creativecommons.org/licenses/by/4.0/>), which permits unrestricted use, distribution, and reproduction in any medium, provided you give appropriate credit to the original author(s) and the source, provide a link to the Creative Commons license, and indicate if changes were made.

## References

- Brezinski, M.E.: *Optical Coherence Tomography: Principles and Applications*. Academic Press, Boston (2006)
- Hirose, K., Liang, Y., Kurosaka, Y., Watanabe, A., Sugiyama, T., Noda, S.: Watt-class high-power, high-beam-quality photonic-crystal lasers. *Nat. Photonics* **8**, 406–411 (2014)
- Imada, M., Noda, S., Chutinan, A., Tokuda, T., Murata, M., Sasaki, G.: Coherent two-dimensional lasing action in surface-emitting laser with triangular-lattice photonic crystal structure. *Appl. Phys. Lett.* **75**(3), 316–318 (1999a)
- Imada, M., Noda, S., Kobayashi, H., Saki, G.: Characterization of a distributed feedback laser with air/semiconductor gratings embedded by the wafer fusion technique. *IEEE J. Quantum Electron.* **35**(9), 1277–1283 (1999b)
- Johnson, S.G., Joannopoulos, J.D.: Block-iterative frequency-domain methods for Maxwell's equations in a planewave basis. *Opt. Express* **8**(3), 173–190 (2001)
- Kawashima, S., Kawashima, T., Nago, Y., Hori, Y., Iwase, H., Uchida, T., Hoshino, K., Numata, A., Uchida, M.: GaN-based surface-emitting laser with two-dimensional photonic crystal acting as distributed-feedback grating and optical cladding. *Appl. Phys. Lett.* **97**, 251112 (2010)
- Kennedy, K., Revin, D.G., Krysa, A.B., Groom, K.M., Wilson, L.R., Cockburn, J.W., Hogg, R.A.: Fabrication and characterization of InP-based quantum cascade distributed feedback lasers with inductively coupled plasma etched lateral gratings. *Jpn. J. Appl. Phys.* **46**, 2424–2428 (2007)
- Kurosaka, Y., Sakai, K., Miyai, E., Noda, S.: Controlling vertical optical confinement in two-dimensional surface-emitting photonic-crystal lasers by shape of air holes. *Opt. Express* **16**(22), 1848–18494 (2008)
- Kurosaka, Y., Iwahashi, S., Sakai, K., Miyai, E., Kunishi, W., Ohnishi, D., Noda, S.: Band structure observation of 2D photonic crystal with various v shaped air hole arrangements. *IEICE Electron. Express* **6**(13), 966–971 (2009)
- Kurosaka, Y., Iwahashi, S., Liang, Y., Sakai, K., Miyai, E., Kunishi, W., Ohnishi, D., Noda, S.: On-chip beam-steering photonic-crystal lasers. *Nat. Photonics* **4**, 447–450 (2010)
- Laws, G., Larkins, E., Harrison, I., Molloy, C., Somerford, D.: Improved refractive index formulas for the Al<sub>x</sub>Ga<sub>1-x</sub>N and In<sub>y</sub>Ga<sub>1-y</sub>N Alloys. *J. Appl. Phys.* **89**, 1108–1115 (2001)
- Lefevre, H.C.: *The Fiber-Optic Gyroscope*. Artech House, London (2014)
- Li, A., Chen, J., Yang, Q., Zhang, Y., Lin, C.: The effect of dispersion of the refractive index on the performance of mid-infrared quantum cascade lasers. *J. Cryst. Growth* **227–228**, 313–318 (2001)
- Mitschke, F.: *Fiber Optics—Physics and Technology*, Chapter 6. Springer, New York (2009)
- Mitsuhashi, Y.: *Optical storage: science and technology*. *Jpn. J. Appl. Phys.* **37**, 2079–2083 (1997)
- Miyai, E., Sakai, K., Okano, T., Kunishi, W., Ohnishi, D., Noda, S.: Lasers producing tailored beams. *Nature* **441**, 946 (2006)

- Nielsen, J.B., Sondergaard, T., Barkou, S.E., Bjarklev, A., Broeng, J., Nielsen, M.B.: Two-dimensional Kagome structure, fundamental hexagonal photonic crystal configuration. *Electron. Lett.* **35**(20), 1736–1737 (1999)
- Noda, S., Yokoyama, M., Chutinan, A., Imada, M., Mochizuki, M.: Polarization mode control of two-dimensional photonic crystal laser by unit cell structure design. *Science* **293**, 1123–1125 (2001)
- Ohnishi, D., Okano, T., Imada, M., Noda, S.: Room temperature continuous wave operation of a surface emitting two dimensional photonic crystal laser. *Opt. Express* **12**(8), 1562–1568 (2004)
- Plihal, M., Maradudin, A.A.: Photonic band structure of two-dimensional systems: the triangular lattice. *Phys. Rev. B* **44**(16), 8565 (1991)
- Sakai, K., Miyai, E., Sakaguchi, T., Ohnishi, T.D., Okano, T., Noda, S.: Lasing band-edge identification for a surface-emitting photonic crystal laser. *IEEE J. Sel. Areas Commun.* **23**(7), 1335–1340 (2005)
- Sakai, K., Miyai, E., Noda, S.: Coupled-wave model for square-lattice two-dimensional photonic crystal with transverse-electric-like mode. *Appl. Phys. Lett.* **89**, 021101 (2006)
- Taylor, R.J.E., Williams, D.M., Childs, D.T.D., Stevens, B.J., Shepherd, L.R., Khamas, S., Groom, K.M., Hogg, R.A., Ikeda, N., Sugimoto, Y.: All-semiconductor photonic crystal surface emitting lasers based on epitaxial re-growth. *IEEE J. Sel. Top. Quantum Electron.* **19**(4), 4900407 (2013a)
- Taylor, R.J.E., Williams, D.M., Orchard, J.R., Childs, D.T.D., Khamas, S., Hogg, R.A.: Band structure and waveguide modelling of epitaxially regrown photonic crystal surface emitting lasers. *J. Phys. D* **46**(26), 264005 (2013b)
- Werlea, P., Slemra, F., Maurera, K., Kormannb, R., Mucke, R., Janker, B.: Near- and mid-infrared laser-optical sensors for gas analysis. *Opt. Lasers Eng.* **37**, 101–114 (2001)
- Williams, D., Groom, K., Childs, D., Taylor, R., Khamas, S., Hogg, R., Stevens, B., Ikeda, N., Sugimoto, Y.: Epitaxially regrown GaAs-based photonic crystal surface emitting laser. *IEEE Photonics Technol. Lett.* **24**(11), 966–968 (2012a)
- Williams, D., Groom, K., Childs, D., Taylor, R., Khamas, S., Hogg, R., Stevens, B., Ikeda, N., Sugimoto, Y.: Optimisation of coupling between photonic crystal and active elements in an epitaxially regrown GaAs based photonic crystal surface emitting laser. *Jpn. J. Appl. Phys.* **51**, 02BG05 (2012b)
- Yokoyama, M., Noda, S.: Polarisation mode control of two-dimensional photonic crystal laser having a square lattice structure. *IEEE J. Quantum Electron.* **39**(9), 1074–1080 (2003)
- Yokoyama, M., Noda, S.: Finite-difference time-domain simulation of two dimensional photonic crystal surface-emitting laser. *Opt. Express* **13**(8), 2069–2080 (2005)